Performance of ammonia fuel in a spark assisted compression Ignition engine

Christine Mounaïm-Rousselle, Adrien Mercier, Pierre Brequigny, Clément Dumand, Jean Bouriot, Sébastien Houillé

HAL Id: hal-03519268
https://hal.science/hal-03519268

Submitted on 10 Jan 2022

Performance of ammonia fuel in a spark assisted compression Ignition engine

Christine Mounaïm-Rousselle[1] , **Adrien Mercier[1], Pierre Brequigny[1], Clément Dumand[2], Jean Bouriot[2] and Sébastien Houillé[2]**

Abstract
Recent studies concluded that the use of ammonia in SI engines is possible thanks to an ignition booster or promoter. In this paper, the improvement of premixed ammonia/air combustion for internal combustion engines is studied as a function of performance and exhaust pollutants in a Spark-Assisted Compression Ignition single-cylinder engine, which supports a higher compression ratio (CR). For the first time, pure NH_3 combustion was performed over a large range of engine operating conditions. The study concludes that neat ammonia can be used over a large operating range, here driven by the intake pressure, using a classical ignition device with a CR of 14–17 at 1000 rpm. The comparison with previous data obtained in a current single-cylinder SI engine clearly shows the potential of this engine mode, even for very low loads and various engine speeds (650, 1000, 2000 rpm), in spite of an initial aerodynamic that is not optimized to enhance flame-turbulence interaction. Kinetic simulations provide some explanations about exhaust emission behaviour, especially unburnt NH_3, H_2, NO_x and N_2O.

Introduction

To reach the carbon neutrality target set for Europe in 2050, decarbonized energies have to replace fossil energies. As recently concluded by MacFarlane et al., ammonia, one of the simplest 'electro-fuels' (*e*-fuels), *'clearly has the potential to become the dominant form of transportable renewable energy in the future, displacing fossil fuel'* in applications[1] such as energy production and/or transportation. Ammonia, considered as a hydrogen carrier, has several advantages over hydrogen itself, such as: a lower cost per unit of stored energy; a higher volumetric energy density; easier and more widespread production, handling and distribution capacity; a better commercial viability; liquid phase obtained by compression to 0.9 MPa at atmospheric temperature; and lastly, a well-established reliable infrastructure for both storage and distribution (including pipeline, rail, road, ship). It is important to emphasize that ammonia is *complementary* to the delivery of the 'Hydrogen Economy', as concluded recently by Valera-Medina et al.[2]

In terms of global efficiency, it will be more advantageous to consider NH_3 directly as fuel combusted in gas turbines, industrial furnaces or internal combustion engines, most likely after partial or complete thermal cracking into nitrogen and hydrogen to balance out its high auto-ignition temperature (a positive safety feature), as recently concluded in different reviews.[3,4]

The idea of using ammonia as an engine fuel is not new, since the first uses in a vehicle date back to the 1930s–1940s (in Norway and Belgium).[5] In the 1960s, several studies focused on the potential of ammonia as a fuel for both gasoline and diesel engines.[6–11] Recently in the 2010s, new vehicle tests were carried out but mainly based on the idea of partially replacing conventional fuel, since the combustion characteristics of

[1]Laboratoire PRISME, Université d'Orléans, Orleans, France
[2]Innovation Department, STELLANTIS-PSA, Paris, France

Corresponding author:
Christine Mounaïm-Rousselle, Laboratoire PRISME, Université d'Orléans, rue Léonard de Vinci, Polytech Vinci, Orleans 45072, France.
Email: christine.rousselle@univ-orleans.fr

Table 1. Main properties of ammonia compared to current engine fuels.

	H_2	NH_3	Gasoline	n-decane
Energy content (MJ/kg)	120.0	18.8	44.0	42.4
Energy density (MJ/l)	4.8	11.5	32.0	35.2
RON (−)	>130	130	95–98	0
Stoichiometric air/fuel (−)	2.4	6.05	15.3	14.3
Laminar flame velocity (ϕ = 1, 298 K, 1 bar) (cm/s)	210	7	≈40	≈45–50
Adiabatic flame temperature (K)	2519	2107	2390	2300

ammonia do not match those of conventional fuels. For example, ammonia is in gaseous phase at ambient pressure and temperature and is in liquid form at 8.5 bar at 20°C. Its volumetric energy density, 11.5 MJ/NL, is about three times lower than that of diesel or half that of ethanol and 30% lower than that of methanol, higher than that of methane and more than twice that of hydrogen. Its boiling temperature is also close to that of LPG for example. Its auto-ignition temperature is very high (650°C), limiting the occurrence of knock but its combustion rate is five times slower than that of conventional spark-ignition engine fuel types. Lastly, depending on the equivalence ratio, its combustion can generate high emissions of NO_x due to the fuel-route or NH_3 slip. Table 1 summarizes the main properties of ammonia fuel in comparison to current engine fuels.

Nonetheless, as underlined in the review by Mounaïm-Rousselle and Brequigny[12] on Spark-Ignition (SI) engines fuelled with NH_3, the low auto-ignition ability of ammonia makes the SI engine the best candidate for pure ammonia operation in order to reach the zero CO_2 emission target for transportation. This is due to the fact that in order to auto-ignite ammonia in a compression ignition engine, an extremely high compression ratio (above 35:1) is required.[13] Due to the unsuitable fuel properties of ammonia for compression ignition, the literature on ammonia alone as fuel in Compression-Ignition (CI) engines is scarce. Most studies have focused on dual-fuel operation as underlined recently in the review by Dimitriou and Javaid.[14] However, even in the case of SI engines, as recently shown in Lhuillier et al.,[15,16] under several operating conditions (low load, low and high engine speed), the self-propagation of an ammonia-air flame is not reachable in current SI engines and a warm-up period with another fuel is needed. At least 5% in volume of H2 is required to guarantee ignition and stable combustion over a large range of operating conditions. In order to extend the operating range of pure ammonia combustion, Garabedian and Johnson[6] highlighted 60 years ago that the conversion of CI engines to spark ignition mode is the '*prominent short-term solution*' due to the higher compression ratio than in an SI engine. Pearsall and Garabedian[8] found that a ratio of 16:1 was the optimum to run with neat ammonia. This is the only previous study on neat Ammonia Spark-Assisted Compression Ignition (SACI) engines.

It was concluded that a large bore, a more concentrated combustion chamber and a more centrally placed spark plug were preferable to optimize the efficiency and therefore decrease the specific fuel consumption. Moreover, a higher power output was reached compared to a diesel or ammonia/diesel blend CI-engine, without the need for supercharging. The present study reports not only new but also the first data on the performance and exhaust gas content in a SACI engine as a function of different parameters such as engine speed, intake pressure and ammonia-air equivalence ratio. The compression ratio was varied from 14:1 to 17:1 to assess the potential of the SACI operating mode as a function of this parameter. The results are compared with previous results obtained in a current SI engine.[17] Chemical kinetics were modelled using the CHEMKIN-PRO package in ANSYS, with the built-in zero-dimensional, two-zone Spark Ignited engine model. This model uses the NH_3 reaction mechanism from Stagni et al.,[18] containing 31 species and 203 reactions, to predict any chemical heat release, including LTHR with a 2-zone model (unburned fuel/air/EGR and burned gases respectively) and to highlight some tendencies of exhaust gases such as NO, NO_2, N_2O and unburnt fuels (NH_3 and H_2).

Experimental method

Experimental setup

Engine experiments were conducted in a single cylinder four-stroke compression ignition engine (DV6F PSA), retrofitted as a Spark-Assisted Compression Ignition engine. A classical cold type spark-plug (NGK ILZKR8C8G), with an Iridium tip on the centre electrode (0.6 mm diameter) and a Platinum ground electrode to limit erosion of the electrode was used with the original inter electrode gap, that is, 0.8 mm. It was not centrally located but implemented on the side near the original location of the injector, in order to favour a flex combustion mode, as shown in Figure 1. The compression ratio was changed from 14:1 to 17:1 by using shims to change the height between the piston and the cylinder head. Decreasing the volume ratio results in an increase in the squish area and probably impacts the wall heat exchange. All the engine specifications are presented in Table 2. Since most of the results will be compared to previous experiments performed in an SI
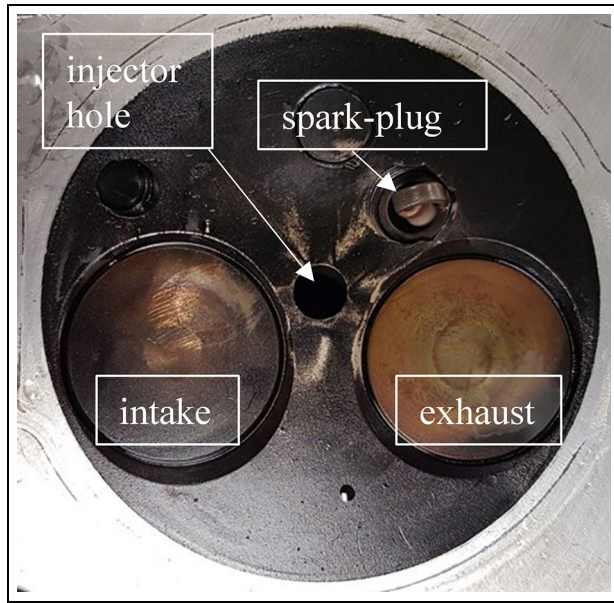
Figure 1. Implementation of the spark plug in a DV6 engine.

Table 2. Engine specifications.

	SACI (DV6)	SI (EP6)[17]
Displaced volume	390 cm³	400 cm³
Stroke	88.3 mm	85.8 mm
Bore	75 mm	77 mm
Connecting rod length	136.8 mm	138.5 mm
Compression ratio	From 14 to 17	10.5
Number of valves	2	4
Swirl ratio (50 CAD BDTC)	2.36	0
Tumble ratio (50 CAD BTDC)	0	2

EP6 single-cylinder engine 17, the specifications of this engine are also listed in the table.

The engine is driven by an electric motor at selected engine speeds varying from 650 to 2000 rpm. Using the optical encoder placed in the main crankshaft, the angular position is monitored with a 0.1 Crank Angle

Degree (CAD) resolution. The in-cylinder pressure measurement is obtained by means of a Kistler piezo-electric pressure transducer (6045A). Intake and exhaust temperature and pressure are monitored using type K thermocouples and piezo-resistive absolute pressure transducers. The absolute in-cylinder pressure is obtained by equalizing it with the mean absolute intake pressure, P_{in}, at 20 CAD after intake valve opening. For all tests, the charge duration for the ignition coil was set to 2 ms. Other durations were tested without any noticeable effect. For all the data presented below, the Spark Ignition Timing (SIT) was optimized with the maximum Indicated Mean Effective Pressure (IMEP) as control parameter, guaranteeing a COV_{IMEP} below 5%.

All gaseous flows are measured and controlled using Brooks thermal mass flowmeters with $\pm$ 0.7% accuracy which guarantee control of the equivalence ratio with 1.5% accuracy. All gases are preheated to the intake temperature and premixed in an intake plenum before intake port injection. A global scheme of the experimental setup is shown in Figure 2.

A 2D view of the mean flow field (computed by means of CONVERGE CFD) 37 CAD Before Top Dead Centre (BTDC) is presented in Figure 3. As it is based on a CI engine, it has to be underlined that the design of the intake port and the combustion chamber, here a re-entrant piston bowl, generates a mean swirl number of 2.

Apparent Heat Release Rate (HRR) is computed from pressure trace post processing with the first law of thermodynamics, as follows:

$$\frac{dQ}{d\theta} = \frac{\gamma}{\gamma - 1} * P * \frac{dV}{d\theta} + \frac{1}{\gamma - 1} V * \frac{dP}{d\theta} \tag{1}$$

where γ is the heat capacity ratio, P, V and θ, the cylinder pressure and volume and crank angle, respectively. Note that heat losses are not considered in the calculation since they are very difficult to determine; they will be the subject of future work. Fuel Mass Burnt (FMB) is then obtained by integrating the heat release and
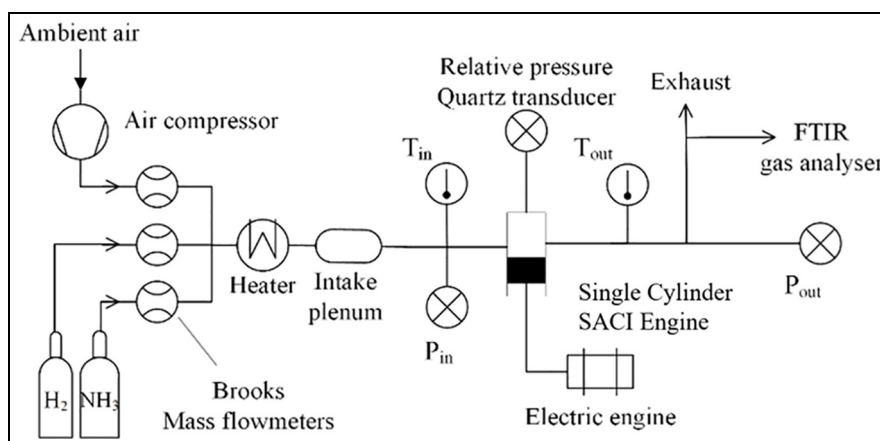

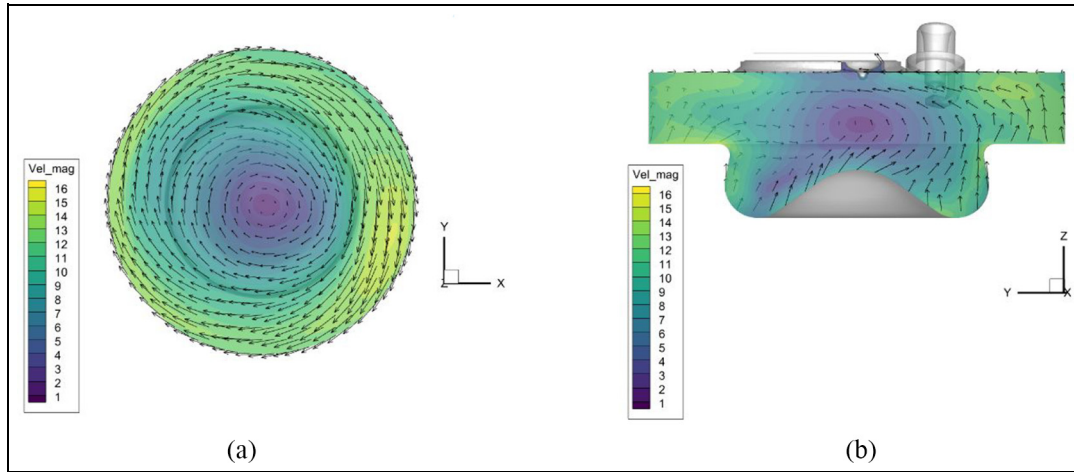**Figure 2.** Layout of the experimental setup.

Figure 3. Example of 2D flow-field (m/s) in a SACI engine at 37 CAD BTDC – 1000 rpm: (a) horizontal cut at middle distance between the cylinder head and the bowl and (b) vertical cut at central line of the chamber (perpendicular to the intake and outlet lines).

apparent HRR is then recalculated using the variable heat capacity ratio computed from the previous FMB. The different phases of combustion propagation were determined by estimating different characteristic timings, named CAXX, which are the Crank Angle degrees corresponding to XX% of the mass burnt fraction. The CA10, CA50 and CA90 are also used as input data, for the built-in zero-dimensional, two-zone Spark Ignited (SI) engine model in Chemkin Pro, to determine the best-fit Wiebe function, since the mass is transferred between the 2 zones at the rate and timing specified by the Wiebe function.

The wet exhaust gases are analyzed using a Gasmet Fourier Transform Infrared (FTIR) spectrometer to assess NO, NO_2, N_2O and NH_3 concentrations. In addition, a thermal conductivity analyzer for H_2 and a paramagnetic analyzer for O_2 are used on a dry exhaust gas sample, that is, without any H_2O and NH_3 content. The water vapour measurement done with the FTIR analyzer is used for wet correction. The accuracy of the H_2 and O_2 analyzers is $\pm 1.5\%$ (range 0%–20% H_2, 0%–21% O_2). To obtain simultaneous quantitative measurement of many gaseous species with a good time resolution and accuracy, the interferences between the species of interest are correctly identified and considered in the analysis settings. The analysis ranges and uncertainty estimation can be found in previous work [15]. Note that error bars are not plotted consistently in order to improve readability but when the values of NH_3 are higher than 2%, the accuracy is only 20%.

Indicated and volumetric efficiencies are computed as follows:

$$\eta_{ind} = \frac{W_{ind}}{Q_{fuel}} \tag{2}$$

where W_{ind} corresponds to the indicated work, and Q_{fuel} the energy content of the mixture:

Table 3. Overview of the operating conditions.

Engine speed (rpm)	(650; 1000; 2000)
Intake temperature (°C)	50
Intake pressure (bar)	(1; 0.8; minimum)
ϕ (−)	(0.9; 1; 1.1)
CR (−)	(17; 16; 15; 14)
Water and oil temperatures (°C)	80

$$\eta_{vol} = \frac{m_{air} + m_{fuel}}{V^* \rho_{mixture}} \tag{3}$$

with

$$\rho_{mixture} = x_{fuel}^* \rho_{fuel} + x_{air}^* \rho_{air} \tag{4}$$

where m_{air} and m_{fuel} are respectively the mass of air and fuel introduced into the cylinder, V the cylinder volume and $\rho_{mixture}$ the mixture density.

Investigated conditions

Only averaged values over 100 cycles are presented in this paper. The range of investigated operating conditions is summarized in Table 3.

For most of the results presented in this study, the Spark Ignition Timing (SIT) was set to ensure the maximum net IMEP with a coefficient of variation of the IMEP over 100 cycles, COV_{IMEP}, lower than 5%.

Results

Combustion development analysis

Effect of compression ratio at 1000 rpm. An example of in-cylinder HRR is presented in Figure 4(a) for the two extreme compression ratios, that is, 17:1 and 14:1, for a stoichiometric ammonia/air fuel mixture and 1 bar and 50°C of intake pressure and temperature respectively.
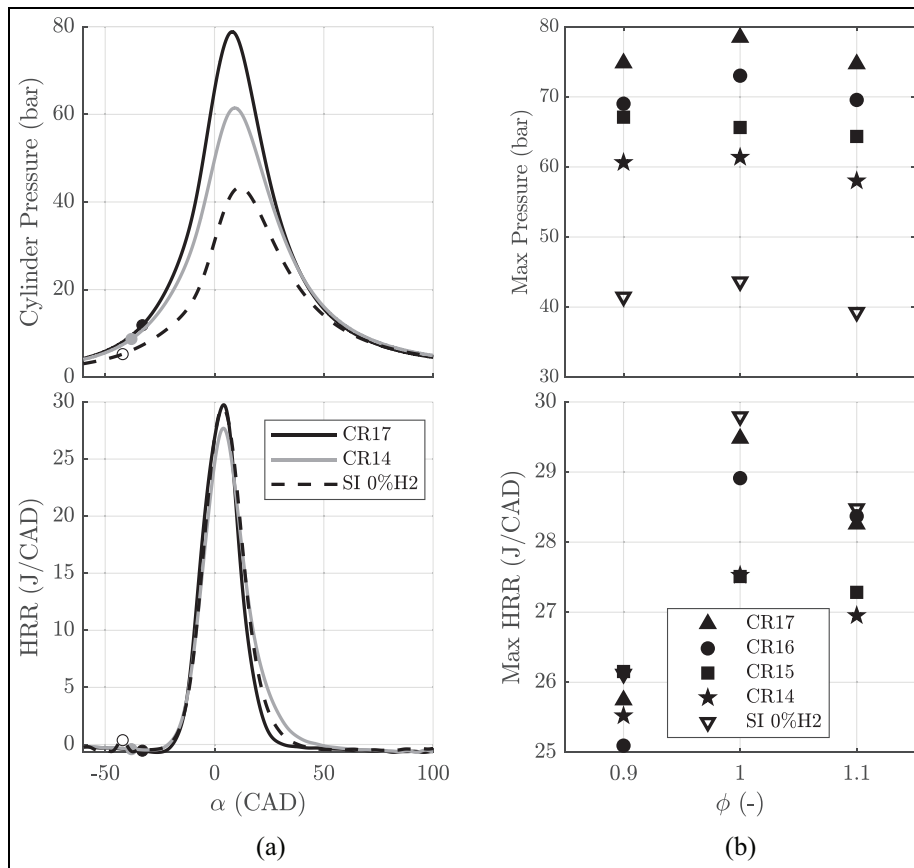
Figure 4. (a) In-cylinder pressure and heat release rate for stoichiometric ammonia/air mixture at CR = 14 and 17, bullet correspond to SIT and (b) max heat release rate and in-cylinder pressure for 4 CR and 3 equivalence ratios Data from SI (0%H2, CR = 10.5:1) – 1000 rpm, Pin = 1 bar, Tin = 50°C.

Data obtained in an SI engine from Mounaïm-Rousselle et al.[17] are plotted for comparison. As expected, in-cylinder pressure decreased with the compression ratio decrease, as highlighted also in Figure 4(b) where the maximum pressure peak is plotted for all CR conditions. However even if HRR also decreased with CR, though slightly, it is clear that the 'SI' HRR is similar to the SACI HRR obtained for the highest CR and not for the lowest one (Figure 4(b)) for three equivalence ratios (slightly lean, stoichiometric and slightly rich). Small deviation of HRR is observed in slightly lean mixture probably due to flame speed reduction. Usually the combustion development considered in SACI mode can be separated into two modes: first the flame development initiated by spark discharge, followed by kinetic combustion as underlined in Hunicz et al.[19] and Olesky et al.[20] However, in the case of ammonia combustion, the two phases are not distinguishable and it can be seen that the combustion development seems similar between SACI and SI since the HRR shape and phasing are very close. This is highlighted by the different combustion phases, displayed in Figure 5, such as early-flame propagation duration (corresponding to the time during which the flame self-propagates without spark assistance), first stage and second stage combustion duration.
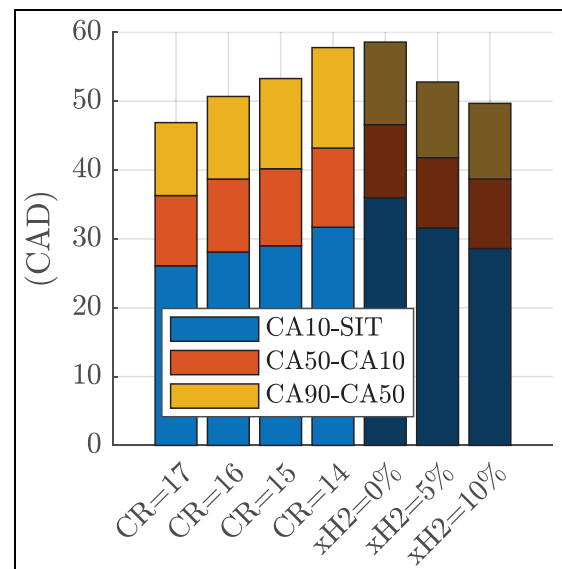

Figure 5. Combustion duration analysis as a function of the compression ratio. Shaded bars for SI engine with different H2% content – 1000 rpm, φ = 1, Pin = 1 bar, Tin = 50°C.

Figure 5 describes these three main combustion phases, represented by CA10-SIT, CA50-CA10 and CA90-CA50 for all CR at 1000 rpm. Only the
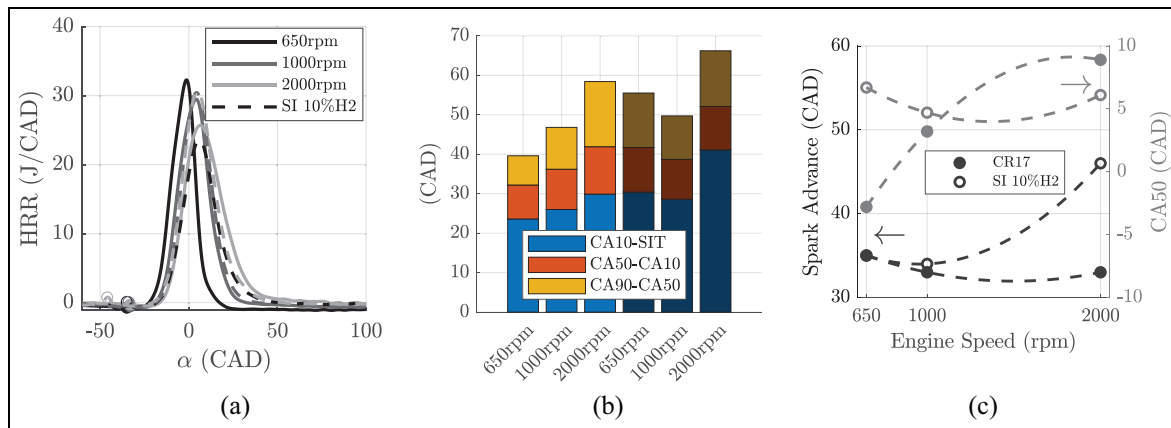
Figure 6. (a) Heat release rate, (b) combustion duration, and (c) combustion phasing for different engine speeds -data in SI with 10% H₂–φ = 1, CR = 17, Pin = 1 bar, Tin = 50°C. Shaded bars for SI engine.

stoichiometric ammonia/air mixture is shown since the tendencies are similar for other equivalence ratios. Shaded bars correspond to previous SI results but with three different H₂ blends (0, 5% and 10% in fuel volume). First, as expected, the higher the CR is, the easier it is to ignite the mixture, since better thermodynamic conditions to ignite ammonia are provided at SIT with high CR. A similar duration can be obtained in an SI engine with an H₂ blend that extends the flammability limit. 'Self-propagation' duration (i.e. the time required from SIT for the flame to be self-propagating) is reduced by 21% and 26% when moving respectively from 14:1 to 17:1 for the SACI mode or from xH₂ = 0%–10% for the SI mode. This induces the same impact on the total combustion duration. However, the comparison between the two engine modes highlights that the total combustion duration, that is, from SIT to CA90, is similar. For example, a CR of 14:1 is required to burn as slowly as the 0% H₂ SI case and the addition of 10% of H₂ offers a similar combustion speed as SACI with a CR of 16:1. However, despite similar total combustion durations, the early flame propagation phase, that is, CA10-SIT, is reduced and global combustion duration, that is, CA90-CA10, is extended in SACI compared to SI. As indicated in Table 2, this is certainly related to the difference in internal flow fields between the two engines: the tumble motion induces turbulent vortices, which help to wrinkle the flame front and thus increase the burning rate, while the swirl motion in a SACI engine does not contribute to flame wrinkling but rather to flame convection, favouring the burning of the mixture in the bowl. Moreover, the fact that the CA90-CA50 phase is the most strongly impacted also suggests that the engine geometry can also affect the burning rate, since some areas are more difficult to burn in a SACI engine. It can also be noted that a compression ratio of 17 for the SACI mode offers the same global combustion duration as that obtained in SI (regardless of the H₂ ratio), due to a higher cylinder temperature, but also to the reduction in the squish

zone which may slow down the flame propagation. Therefore, even if the combustion durations are similar, the combustion stability is better and thus a wider operating range is reached with SACI without any obvious change in the combustion processes.

Effect of engine regime at constant compression ratio. In Figure 6(a), the HRR are plotted as a function of the engine speed for SACI with a CR 17:1, as well as those for an SI engine with 10% of H₂. As expected in the case of the SI mode, since the turbulent intensity increases with engine speed, the time reduction in the combustion stroke due to the increase in engine speed is compensated by the increase in turbulent flame speed. Nonetheless, in SACI mode, the HRR is delayed as a function of the rpm increase and its duration increases. The comparison of the different combustion phases, plotted in Figure 6(b), shows that the time for early flame propagation and combustion development are similar at 1000 rpm for both engines. Yet, due to the different combustion processes, the CA10-SIT in the SACI engine remained quite constant while it increases by 30% when the engine speed increased from 1000 to 2000 rpm in the SI engine. This means that the increase in of the thermodynamic conditions at SIT (even though SIT is being advanced) which might accelerate the kernel flame does not compensate for the engine speed increase. The fact that the total combustion duration was lower at 2000 rpm in the SACI engine than in the SI one suggests that the limitation on the maximum possible engine speed is extended with the SACI concept.

Sensitivity of the spark-ignition timing. To highlight the sensitivity of the ammonia-only SACI combustion process and therefore its stability, an example of this sensitivity to the SIT is presented in Figure 7 for the following conditions: 1500 rpm, with a 0.85 ammonia/air equivalence ratio and 1.08 bar and 30°C of intake pressure and temperature respectively. Faster combustion was
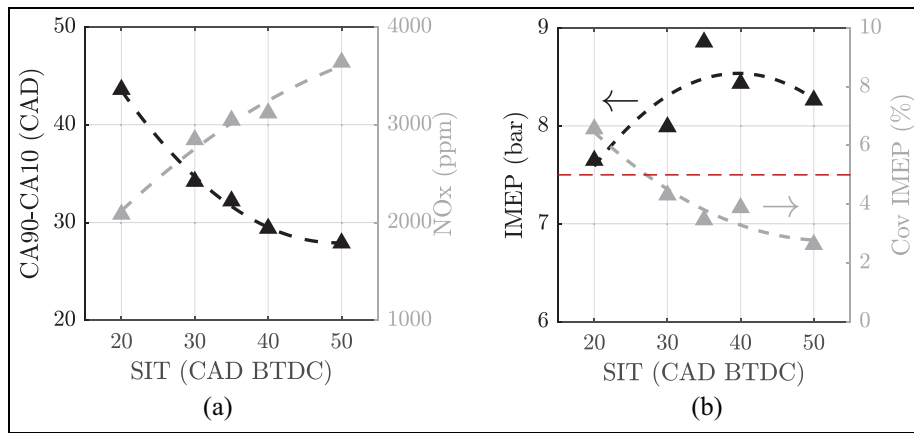
Figure 7. (a) Combustion duration and NO$_x$ emissions and (b) IMEP and COV$_{IMEP}$–ϕ = 0.85, 1500 rpm, 1.08 bar, SACI CR 17:1 and SIT = 40 CADBTDC.
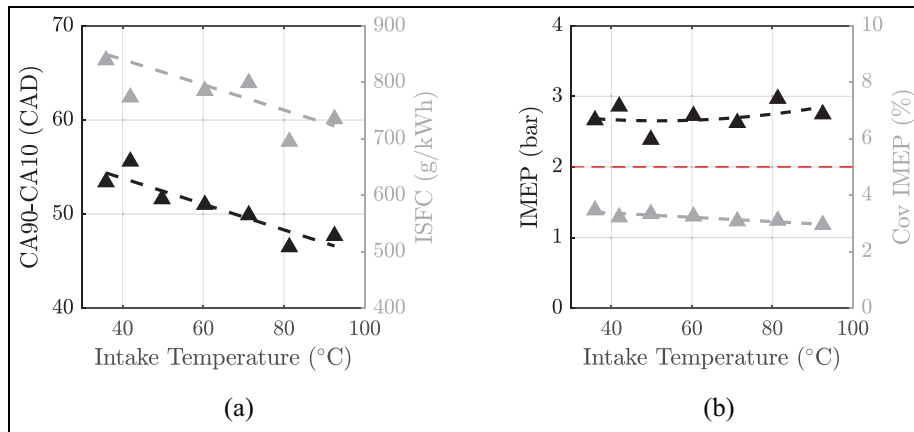

Figure 8. (a) Combustion duration and specific consumption and (b) IMEP and stability as a function of the intake temperature-ϕ = 1, 1500 rpm, Pintake = 0.5 bar in SACI.

obtained, that is, a 30% decrease in total combustion duration was obtained when the SIT varied from 20 to 50 CAD BTDC. However, the best IMEP, that is, the best efficiency, was obtained at SIT = 35 CAD BTDC in Figure 7(b), probably because beyond 35, wall heat losses become dominant. It has to be noted that better stability was achieved with the advancement of the SIT. Therefore, the optimum SIT is based in this study on two criteria: the best IMEP with COV$_{IMEP}$ lower than 5%. It has to be noted also that the SIT strongly affects the NO$_X$ exhaust emissions which almost double in line with the maximum in-cylinder pressure.

Intake temperature effect. Intake temperature variation experiments were performed at 1500 rpm, for a stoichiometric ammonia-air mixture, at low load (namely 0.5 bar intake pressure). As expected, results show that the increasing intake temperature induces a shorter combustion duration due to the increased flame speed leading to an improved efficiency, as shown in Figure 8(a), and this with a constant ignition phasing set to 40

CADBTDC. Notwithstanding a lower ISFC, Figure 8(b) shows only a slight IMEP increase since the energy introduced is reduced due to a lower intake gas density. Finally, combustion stability is improved showing the possible extension of the following low-load operating limits at high temperatures.

Operating limits

In Figure 9, the IMEP obtained for the load operating limits, that is, the minimum intake pressure with maintained stability, is plotted for three equivalence ratios and all compression ratios. For comparison, the operating limits previously obtained in an SI engine are also shown, either with neat ammonia or ammonia slightly doped with hydrogen. The intake temperature was fixed at 50°C, with optimized SIT, in accordance with the criteria presented in section 4.1.3. First, it is clear that the lower engine operating limit is significantly extended with a SACI engine compared to a SI engine: even if promoting the combustion with H$_2$ addition offers a lower minimum intake pressure, it does not
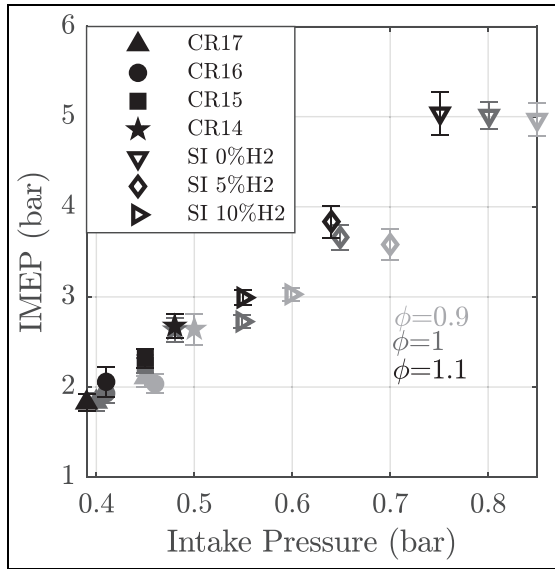
Figure 9. Minimum IMEP versus minimum intake pressure at 1000 rpm – Tin = 50°C.

result in a level as low as the one reached with the SACI engine at the lowest CR (14:1). By increasing the compression ratio, a lower load can be reached. In fact, the increase in the in-cylinder temperature due to the higher compression ratio facilitates the flame development, thus increasing the engine stability and then allowing a lower intake pressure and IMEP. The maximum in-cylinder temperature was obtained for slightly rich mixtures offering a shorter combustion duration, in agreement with Lhuillier et al.,[21] an improved combustion stability and thus, a lower intake pressure limit. Notwithstanding a lower intake pressure, IMEP did not vary much when moving from a lean to a rich mixture due to a higher heating value of the mixture.

Figure 10(a) indicates the minimum IMEP that guarantees stable operation, that is, $COV_{IMEP} < 5\%$,

as a function of the engine speed and equivalence ratio. The optimum was obtained at low engine speed, due to the low effect of turbulence on flame speed using a diesel engine type, since the effect of the engine speed on the angular range over which combustion takes place is greater than that of turbulence. Despite a lower intake pressure obtained at 1000 rpm and near $\phi = 1.1$, one can notice an area of constant IMEP between 650 and 1000 rpm for slightly rich mixtures (Figure 10(b)). Indeed, the optimum volumetric efficiency is at 1000 rpm while indicated efficiency increases with engine speed because of the limited heat exchanges despite a reduced combustion window as highlighted in Figure 11. From these results on these operating conditions, both efficiencies are improved with the SACI mode.

In Figure 12, the IMEP obtained for the load operating limits is plotted for the three equivalence ratios and the three engine speeds (650, 1000 and 2000 rpm) at CR 17:1. A similar trend to that shown in Figure 9 is obtained, that is, a wider operating range with the SACI operating mode, even if up to 10% of H_2 is used to help combustion in the SI operating mode, and better stability is obtained in a slightly rich mixture.

Effect of compression ratio on pollutant emissions

Among the operating conditions presented in Table 3, the pollutant emissions analysis focused only on the operating points with an intake pressure of 1 bar and the comparison with SI engine results was conducted with neat ammonia combustion only.

Figure 13 presents H_2 and NH_3 exhaust emissions as a function of the equivalence ratio and CR. The tendency is similar for both as already observed in Mounaïm-Rousselle et al.,[17] that is, an increase in H_2 exhaust emissions with the equivalence ratio. The variation of hydrogen exhaust emissions as a function of CR
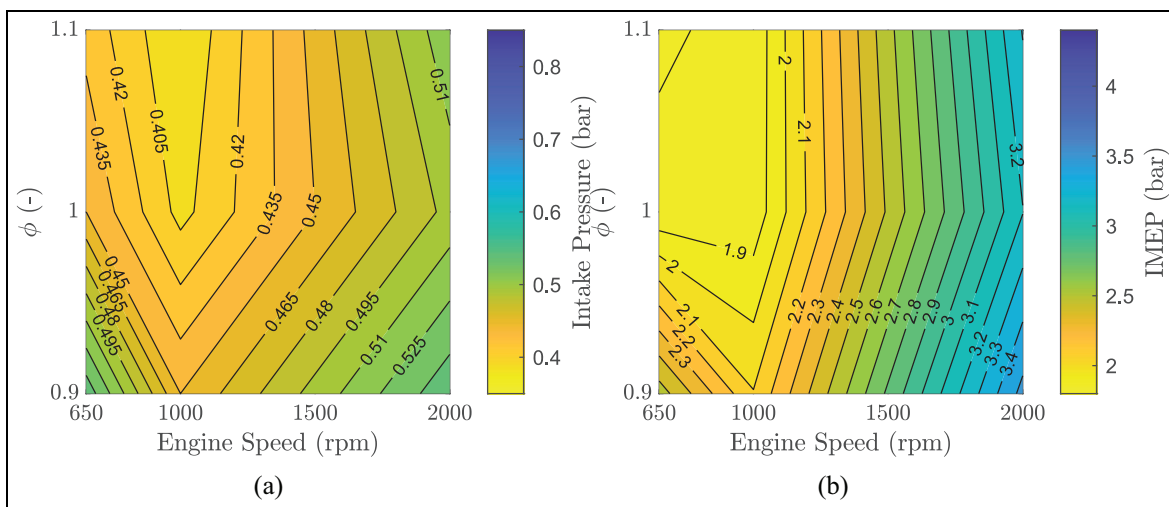

Figure 10. (a) 2D plot of minimim intake pressure limit and (b) 2D plot of corresponding IMEP as a function of engine speed and equivalence ratio – CR = 17:1, Tin = 50°C, Pin = 1 bar.

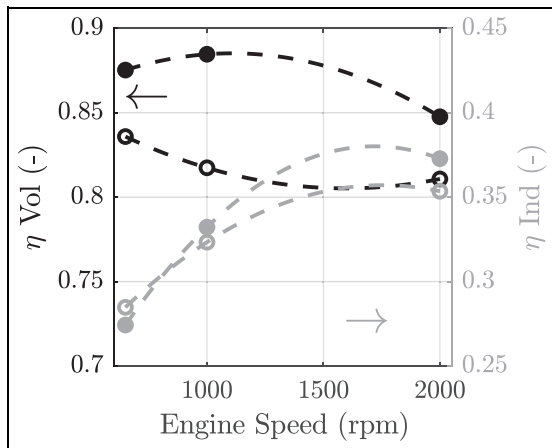**Figure 11.** Volumetric and indicated efficiencies as function of engine speed – CR = 17:1, φ = 1, Pin = 1 bar, Tin = 50°C. Empty symbol = SI engine with 10% H₂.

Figure 13. Ammonia and hydrogen exhaust emissions at 1000 rpm for different CR – comparison with H₂ values predicted by kinetics simulation with the STAGNI mechanism at 100 CAD ATDC.
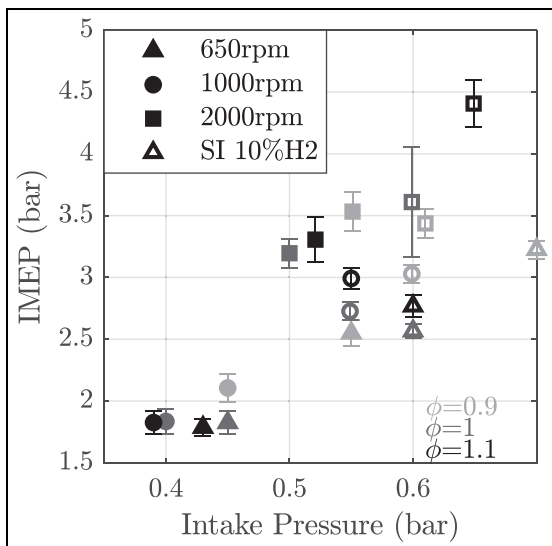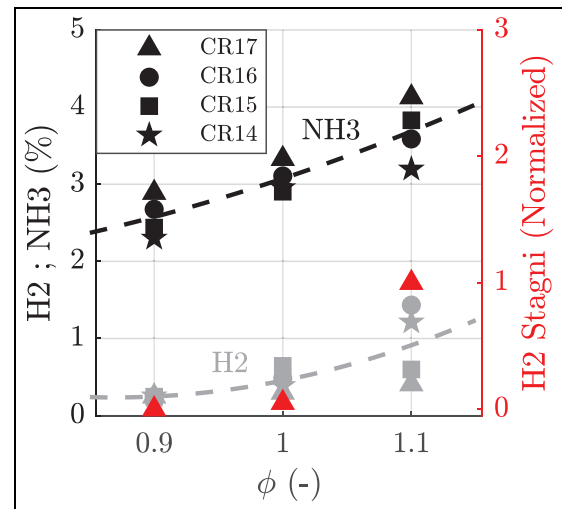

Figure 12. Minimum IMEP versus minimum intake pressure for three engine speeds – CR = 17:1, Tin = 50°C. Previous data in SI engine with 10% H₂.

is not so clear. Furthermore, results from the kinetics simulation (Figure 14) indicate an identical end-cycle hydrogen level for all CR although the maximum level of hydrogen formed during the combustion process is higher for high CR, no doubt due to the temperature increase. It is striking to see that even for a slightly rich mixture no unburnt NH_3 emission is predicted by the kinetics simulation as NH_3 is totally dissociated into H_2 at these conditions. It is then clear that unburned ammonia emissions are mainly due to the fuel trapped in the crevices. Therefore, unburned ammonia emissions increased linearly with CR, in accordance with the unburned fuel mechanism presented in Westlye et al.[22]

As can be seen in Figure 15 where NO_x emissions are plotted as a function of unburned NH_3 emissions, the

maximum of NO_x emissions is obtained for a lean mixture (here $\phi = 0.9$) as expected. Despite the increase in the mean combustion chamber temperature as a function of CR increase, NO_x emissions are not really affected by CR since the thermal NO_x pathway is not the dominant one in the case of pure ammonia combustion, as underlined in Mounaïm-Rousselle et al.[17] and Westlye et al.[22] NO_x emissions are reduced by approximately 20% in a lean mixture and even more at stoichiometry when switching from SI to SACI, although max HRR are very similar in the two engines in a lean mixture as already presented in Figure 4(a). Because the majority of NO emissions come from the NO fuel route, it can be assumed that the lower combustion efficiency in SACI makes less N available from the fuel to form NO. One can however note that NO_x emission is below 500 ppm for a stoichiometric ammonia/air mixture in the case of SACI. The comparison with previous data on an SI engine (Figure 15) indicates a strong increase in NH_3 emissions, respectively + 270% between SACI with CR 17:1 and SI with 0% of hydrogen (even if the accuracy of NH_3 emissions decreases strongly at high values). Furthermore, extrapolated exhaust NH_3 for SACI with a CR of 10,5:1 still gives a higher exhaust NH_3 level, this can be attributed to the engine geometry, explained by the trapping of NH_3 during the compression stroke in the squish zone and/or in the crevices and the later release of this NH_3 which cannot burn later in the cycle, but also by a higher maximum cylinder pressure due to higher CR as mentioned before.

As the third greenhouse gas in the world, N_2O (nitrous oxide) plays an important role in global warming. Its warming impact is about 270 times greater than that of carbon dioxide over a century.[23] In Figure 16(a), N_2O emissions are plotted as a function of the equivalence ratio for different CR. As already
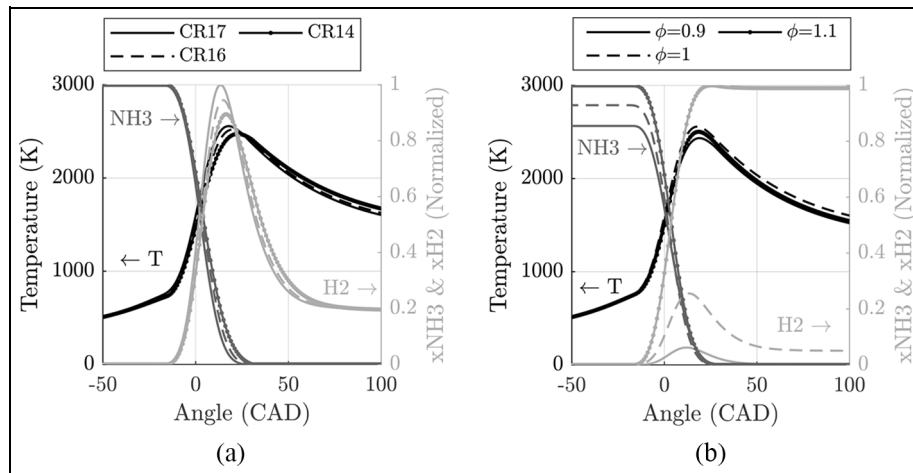
Figure 14. Evolution of average chamber temperature and NH$_3$ and H$_2$ fractions estimated by kinetics simulation using Stagni mechanism: (a) for different CR at ϕ = 1 and (b) for different equivalence ratios at CR = 17:1.
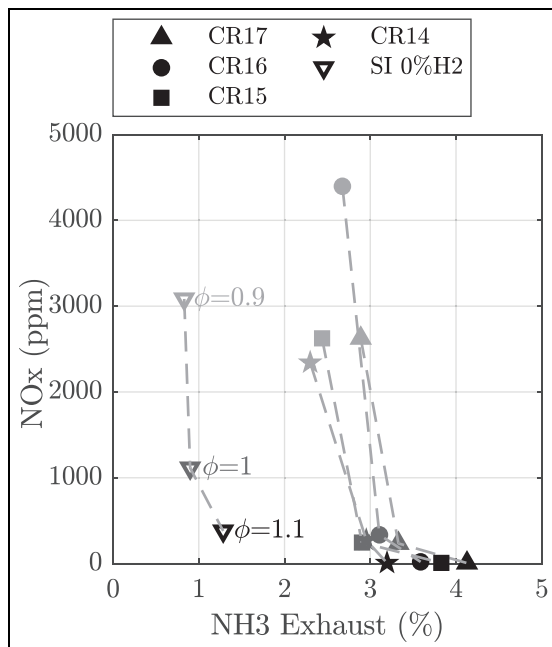

Figure 15. NO$_x$ -NH$_3$ emission 1bar as a function of CR − 1000 rpm, Pin = 1 bar.

mentioned in Mounaïm-Rousselle et al.,[17] the emission decreases as a function of the increase in the equivalence ratio since, following the low temperature N$_2$O formation mechanism presented in Westlye et al.,[22] N$_2$O can be formed from NO$_2$ and NH$_2$. Therefore, if NH$_3$ from crevices is released during the expansion stroke with a sufficient amount of O$_2$, NH$_2$ and thus N$_2$O are formed. This is the reason why N$_2$O levels are higher in a lean mixture. On the other hand, although higher ammonia unburned emissions are found with high CR (Figure 13), since the end of the combustion occurs earlier in the cycle, the temperature in the expansion phase is lower (Figure 16(b)), leading to a partial freezing of the reaction and thus a slight decrease in N$_2$O emissions. However, global low levels below 50 ppm are found, which corresponds in equivalence to

the global warming impact of 1.3% of CO$_2$ and are of the same order of magnitude as the N$_2$O levels shown in Westlye et al.[22] Even though unburned ammonia cannot be predicted by a 0D model, a similar trend to the values predicted by the kinetic simulation and measurement is observed since NO$_x$ and O$_2$ are preponderant in lean mixtures.

In Figure 17, NOx emissions which include NO and NO$_2$ emissions mostly consist of NO, that is, > 95%, for the SACI mode, contrary to the previous data obtained in an SI engine where more than 40% of NO$_2$ was obtained at ϕ = 1. This ratio is also similar for all CR and equivalence ratios except 1.1 where no NOx emissions were recorded. The following two underlying assumptions can be made: first, the uniformity of the temperature avoids the freezing of the NO$_2$ to NO conversion reaction, as explained in Westlye et al.[22] since the combustion process is similar to the one observed in an SI engine; secondly, since NO$_2$ chemistry is linked with that of N$_2$O, the majority of NO$_2$ could be consumed to form N$_2$O.

Conclusion

Since the initial suggestion made in the 1960s, the present study is the first to focus on the potential a SACI engine to run with an ammonia-air premixture for many operating conditions. The influence of CR on the combustion process, operating limits and pollutant emissions has been pointed out, without any optimization of the spark device. In most cases, the results have been compared to those obtained in a current SI engine.

The main conclusions are the following :

1. By increasing the compression ratio, the change in thermodynamic conditions at spark-ignition timing leads to a lower early flame propagation duration, in comparison to an SI engine. It has to be noted that although the flowfield in a SACI engine is not optimized for premixed flame combustion propagation,
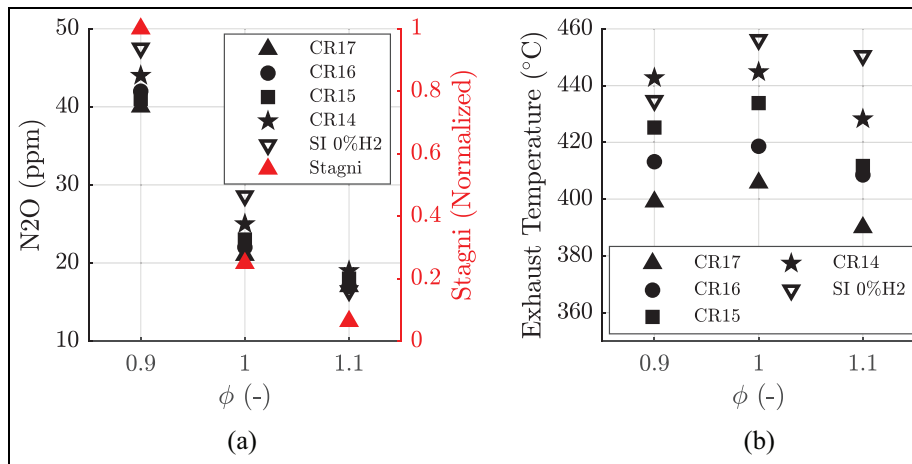
Figure 16. (a) N_2O emissions as a function of equivalence ratios for different CR – 1000 rpm, Pin = 1 bar – values from kinetics simulation at CR 17:1 at 100 CAD ATDC and (b) exhaust temperature as a function of equivalence ratio for all CR – 1000 rpm, Pin = 1 bar.
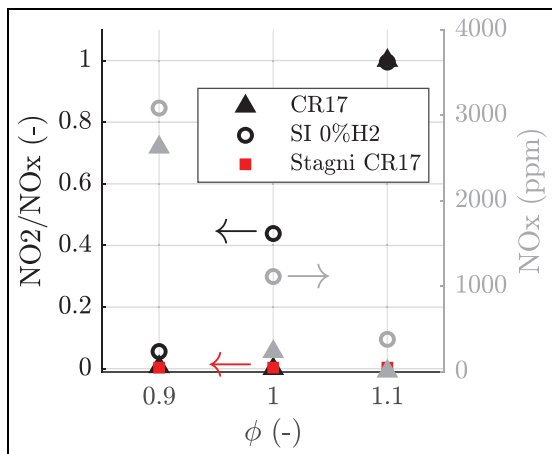

Figure 17. NO_2/NO_x ratio and NO_x emissions as a function of equivalence ratio – 1000 rpm, Pin = 1 bar and CR 17:1. Comparison with NO_2/NO_x ratio values predicted by kinetics simulation with the STAGNI mechanism at 100 CAD ATDC.

a similar flame propagation duration was found between the SACI and SI modes. Therefore, the improvement in early flame propagation in the SACI mode plays an important role in the combustion process and stability, extending the operating range at low loads for SACI compared to SI conditions.

2. An increase in engine speed generates a quasi linear increase in combustion duration for the SACI engine. Nonetheless, the increase in the combustion duration remains limited. On the other hand, a non linear trend is observed for the SI configuration and despite a faster combustion speed at 1000 rpm, combustion is highly degraded at 2000 rpm. Therefore, one can assume that the maximum engine speed limit (not reached in the present study) is increased in SACI.

3. Similar trends concerning pollutant emissions were found between the two engine configurations.

Unburned NH_3 emissions are higher in the SACI mode, increasing with the CR due to the increase in ammonia trapped in the crevices. Besides, the chemical kinetics simulation helped to understand that except for trapped ammonia, for the present temperature conditions, most of the remaining ammonia is dissociated into hydrogen and might increase with CR since the temperature increases as well. N_2O emissions never exceeded 50 ppm, as previously observed for the SI mode, although the ratio increases slightly in a lean mixture.

Finally, the present study indicates that even without modifying the combustion chamber design, the SACI combustion mode is beneficial for NH_3 combustion due to the increase in the compression ratio which makes it possible to reach thermodynamic conditions that facilitate the combustion of NH_3. However, it is clear that future studies are required to better understand the improvement in the combustion process by means of visualization and CFD modelling. Lastly, further studies have to be conducted at higher engine speeds/loads with an optimized ignition device in order to enhance the potential of Ammonia SACI, by considering both efficiencies and NH_3/NOx trade-offs.

Declaration of conflicting interests

Funding

ORCID iD

Christine Mounaïm-Rousselle https://orcid.org/0000-0001-9619-7001

References

1. MacFarlane DR, Cherepanov PV, Choi J, et al. A Roadmap To The Ammonia Economy. *Joule* 2020; 4: 1–20.
2. Valera-Medina A, Xiao H, Owen-Jones M, et al. Ammonia for power. *Prog Energy Combust Sci* 2018; 69: 63–102.
3. Rouwenhorst KHR, Elishav O, Mosevitzky Lis B, et al. Future trends. In: Valera-Medina V and Banares-Alcantara R (eds) *Techno-economic challenges of green ammonia as an energy vector*. Amsterdam: Elsevier, 2021, pp.303–319.
4. Valera-Medina A, Amer-Hatem F, Azad AK, et al. Review on ammonia as a potential fuel: from synthesis to economics. *Energy Fuels* 2021; 35(9): 6964–7029.
5. Koch E. Ammonia as a fuel for motor buses. *J Inst Pet* 1949; 31: 21–32.
6. Garabedian C and Johnson J. *The theory of operation of an ammonia burning internal combustion engine*. Report Fort Belvoir, VA: Defense Technical Information Center, 634681, 1965.
7. Cornelius W, Huellmantel LW and Mitchell HR. Ammonia as an engine fuel. SAE paper 650052, 1965.
8. Pearsall TJ and Garabedian CG. Combustion of anhydrous ammonia in diesel engines. SAE paper 670947, 1967.
9. Sawyer RF, Starkman ES, Muzio L and Schmidt W. Oxides of nitrogen in the combustion products of an ammonia fueled reciprocating engine. SAE paper 680401, 1968.
10. Starkman ES, Newhall HK, Sutton R, et al. Ammonia as a diesel engine fuel: theory and application. SAE paper 670946, 1967.
11. Starkman ES, Newhall HK, Sutton R, Maguire T and Farbar L. Ammonia as a spark ignition engine fuel: theory and application. SAE paper 660155, 1966.
12. Mounaïm-Rousselle C and Brequigny P. Ammonia as fuel for low-carbon spark-ignition engines of tomorrow's passenger cars. *Front Mech Eng* 2020; 6: 70.
13. Gray JTJ, Dimitroff E, Meckel NT and Quillian R. Ammonia fuel – engine compatibility and combustion. SAE paper 660156, 1966.
14. Dimitriou P and Javaid R. A review of ammonia as a compression ignition engine fuel. *Int J Hydrog Energy* 2020; 45: 7098–7118.
15. Lhuillier C, Brequigny P, Contino F and Rousselle C. Performance and emissions of an ammonia-fueled si engine with hydrogen enrichment. SAE paper 2019-24-0137,2019.
16. Lhuillier C, Brequigny P, Contino F and Rousselle C. Combustion characteristics of ammonia in a modern spark-ignition engine. SAE paper 2019-24-0237, 2019.
17. Mounaïm-Rousselle C, Brequigny P, Houillé S and Dumand C. Potential of Ammonia as future Zero-Carbon fuel for future mobility: working operating limits for Spark-Ignition engines. In: *SIA Powertain & energy 2020*. France: Online Digital Platform, 2020. https://hal.archives-ouvertes.fr/hal-03188481
18. Stagni A, Cavallotti C, Arunthanayothin S, et al. An experimental, theoretical and kinetic-modeling study of the gas-phase oxidation of ammonia. *React Chem Eng* 2020; 5: 696–711.
19. Hunicz J, Mikulski M, Koszałka G and Ignaciuk P. Detailed analysis of combustion stability in a spark-assisted compression ignition engine under nearly stoichiometric and heavy EGR conditions. *Appl Energy*; 280: 115955.
20. Olesky LKM, Middleton RJ, Lavoie GA, Wooldridge MS and Martz JB. On the sensitivity of low temperature combustion to spark assist near flame limit conditions. *Fuel* 2015; 158: 11–22.
21. Lhuillier C, Brequigny P, Contino F and Mounaïm-Rousselle C. Experimental study on ammonia/hydrogen/air combustion in spark ignition engine conditions. *Fuel* 2020; 269: 117448.
22. Westlye FR, Ivarsson A and Schramm J. Experimental investigation of nitrogen based emissions from an ammonia fueled SI-engine. *Fuel* 2013; 111: 239–247.
23. Myhre G, Shindell D and Pongratz J. Anthropogenic and natural radiative forcing. In: Stocker T (ed.) *Climate change 2013: the physical science basis; Working Group I contribution to the fifth assessment report of the Intergovernmental Panel on Climate Change*. Cambridge: Cambridge University Press, 20104, pp.659–740.

Appendix

Notation

LPG	Liquified Petroleum Gas
SI	Spark Ignition
CI	Compression Ignition
SACI	Spark Assisted Compression Ignition
CR	Compression Ratio
CAD	Crank Angle Degree
IMEP	Indicated Mean Effective Pressure
HRR	Heat Release Rate
FMB	Fuel Mass Burnt
CAXX	CAD corresponding to XX% of FMB
FTIR	Fourier Transformed Infrared
SIT	Spark Ignition Timing
Pin	Intake Pressure
Tin	Intake Temperature
ISFC	Indicated Specific Fuel Consumption